Accepted Manuscript

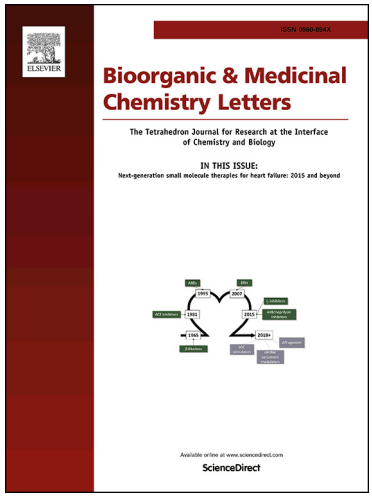

Unexpected Equivalent Potency of a Constrained Chromene Enantiomeric Pair Rationalized by co-Crystal Structures in Complex with Estrogen Receptor Alpha

Birong Zhang, James R. Kiefer, Robert A. Blake, Jae H. Chang, Steven Hartman, Ellen Rei Ingalla, Tracy Kleinheinz, Vidhi Mody, Michelle Nannini, Daniel F. Ortwine, Yingqing Ran, Amy Sambrone, Deepak Sampath, Maia Vinogradova, Yu Zhong, Jerome C. Nwachukwu, Kendall W. Nettles, Tommy Lai, Jiangpeng Liao, Xiaoping Zheng, Hai Chen, Xiaojing Wang, Jun Liang

PII: S0960-894X(19)30057-5
DOI: https://doi.org/10.1016/j.bmcl.2019.01.036
Reference: BMCL 26273

To appear in: *Bioorganic & Medicinal Chemistry Letters*

Received Date: 13 December 2018
Revised Date: 24 January 2019
Accepted Date: 30 January 2019

Please cite this article as: Zhang, B., Kiefer, J.R., Blake, R.A., Chang, J.H., Hartman, S., Ingalla, E.R., Kleinheinz, T., Mody, V., Nannini, M., Ortwine, D.F., Ran, Y., Sambrone, A., Sampath, D., Vinogradova, M., Zhong, Y., Nwachukwu, J.C., Nettles, K.W., Lai, T., Liao, J., Zheng, X., Chen, H., Wang, X., Liang, J., Unexpected Equivalent Potency of a Constrained Chromene Enantiomeric Pair Rationalized by co-Crystal Structures in Complex with Estrogen Receptor Alpha, *Bioorganic & Medicinal Chemistry Letters* (2019), doi: https://doi.org/10.1016/j.bmcl.2019.01.036

Unexpected Equivalent Potency of a Constrained Chromene Enantiomeric Pair Rationalized by co-Crystal Structures in Complex with Estrogen Receptor Alpha

Birong Zhang[a*], James R. Kiefer[a], Robert A. Blake[a], Jae H. Chang[a], Steven Hartman[a], Ellen Rei Ingalla[a], Tracy Kleinheinz[a], Vidhi Mody[a], Michelle Nannini[a], Daniel F. Ortwine[a], Yingqing Ran[a], Amy Sambrone[a], Deepak Sampath[a], Maia Vinogradova[a], Yu Zhong[a], Jerome C. Nwachukwu[b], Kendall W. Nettles[b], Tommy Lai[c], Jiangpeng Liao[c], Xiaoping Zheng[c], Hai Chen[c], Xiaojing Wang[a], Jun Liang[a*]

a. Genentech Inc., 1 DNA Way, South San Francisco, California, 94080, USA
b. Department of Integrated Structural and Computational Biology, The Scripps Research Institute, 130 Scripps Way, Jupiter, FL 33458, USA
c. WuXi AppTec, 288 Fute Zhong Road, Waigaoqiao Free Trade Zone, Shanghai, 200131, China

Graphic Abstract

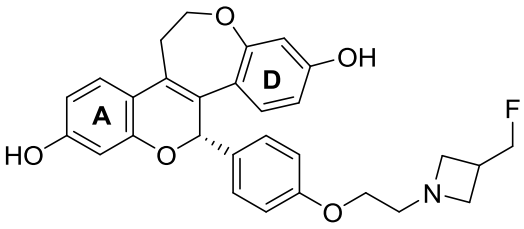

16aa (yellow, default binding mode)
ERα Degradation IC_{50}: 0.055 nM, S_{inf}: 96%

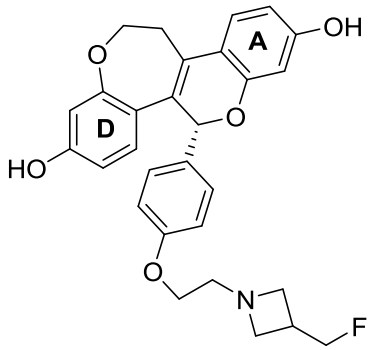

16ab (magenta, flipped binding mode)
ERα Degradation IC_{50}: 0.059 nM, S_{inf}: 93%

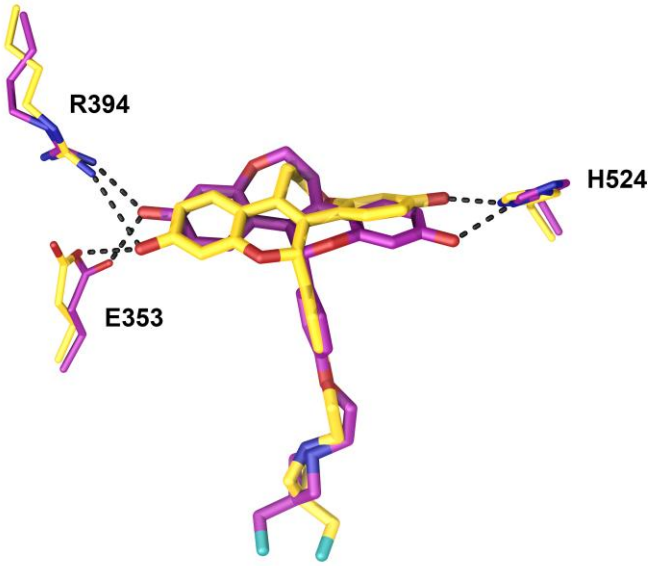

ABSTRACT

Despite tremendous progress made in the understanding of the ERα signaling pathway and the approval of many therapeutic agents, ER+ breast cancer continues to be a leading cause of cancer death in women. We set out to discover compounds with a dual mechanism of action in which they not only compete with estradiol for binding with ERα, but also can induce the degradation of the ERα protein itself. We were attracted to the constrained chromenes containing a tetracyclic benzopyranobenzoxepine scaffold, which were reported as potent selective estrogen receptor modulators (SERMs). Incorporation of a fluoromethyl azetidine side chain yielded highly potent and efficacious selective estrogen receptor degraders (SERDs), such as **16aa** and surprisingly, also its enantiomeric pair **16ab**. Co-crystal structures of the enantiomeric pair **16aa** and **16ab** in complex with ERα revealed default (mimics the A-D rings of endogenous ligand estradiol) and core-flipped binding modes, rationalizing the equivalent potency observed for these enantiomers in the ERα degradation and MCF-7 anti-proliferation assays.

Keywords:

ERα

Estrogen receptor degrader

SERD

Constrained chromene

Estrogen receptor alpha (ERα), an estrogen-dependent nuclear transcription factor,[1] is a well validated therapeutic target for the treatment of estrogen receptor positive (ER+) breast cancer (BC).[2] The FDA-approved drug tamoxifen (**1**) and its active metabolite 4-hydroxytamoxifen (**2**) are SERMs.[3] SERMs compete with the endogenous ligand 17β-estradiol (E_2) and function as antagonists in breast and uterus tissues while acting as agonists in bone cells and lipid metabolism.[4] Despite many BC patients initially responding to tamoxifen, resistance to treatment often occurs.[5] Consequently, ERα degradation has emerged as a new mechanism for inhibiting growth of ERα-dependent tumors.[6] Fulvestrant (**3**), originally designed as a full antagonist, was approved to treat ER+ advanced or metastatic BC, and was later determined to be a SERD.[7] However, clinical efficiency of fulvestrant is limited by its poor pharmacokinetic and pharmaceutical properties.[8] We thus aimed to identify an orally bioavailable SERD for which ERα degradation efficiency was optimized. Due to the remarkable conformational flexibility of the ERα, many structurally diverse SERMs can be accommodated in the ligand binding domain (LBD). We envisioned a rational approach would be to design novel SERDs based on known SERM templates. An example of this approach was the discovery of a potent SERD (**4**, GDC-0927, Figure 1) by researchers at Seragon.[9] Compound **4** demonstrated robust tumor growth inhibition in a mouse xenograft breast cancer tumor model which is resistant to

tamoxifen treatment. Other researchers have developed a series of tetracyclic chromene-derived benzopyranobenzoxepines, such as **5** (Figure 1), to maintain the conformation of the D-ring.[10] Compound **5** was found to be a potent SERM that behaved as a full antagonist in uterus and an agonist in bone cells, plasma lipid metabolism and vagina.[10] The degree of ERα degradation by fulvestrant, **4,** and **5** is depicted in Figure 2 by the maximum percentage change in ERα protein (S_{inf}) at high drug concentrations in an ERα high-content fluorescence imaging assay (Supplementary Method 1). Compound **4** achieved almost the same level of ERα degradation efficiency as fulvestrant (97% of fulvestrant control), while **5** displayed much less degradation efficiency (64%). Herein, we describe our effort in optimizing the degradation efficiency of **5** and the interesting binding modes of a pair of enantiomers based on co-crystal structures.

Figure 1. Known ER ligands

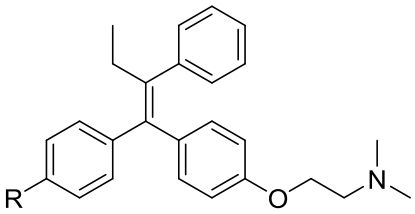

1: R = H: Tamoxifen
2: R = OH: 4-Hydroxytamoxifen

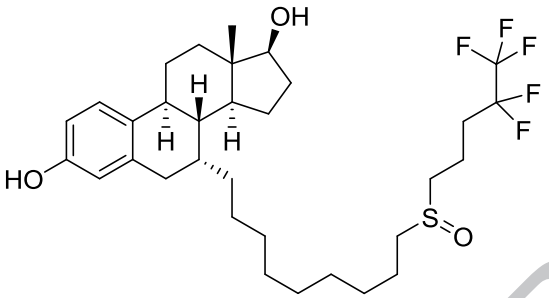

3: Fulvestrant

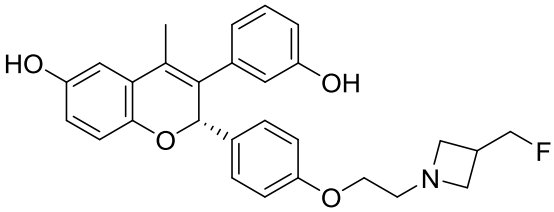

4: GDC-0927

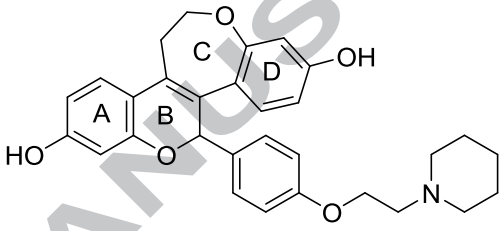

5

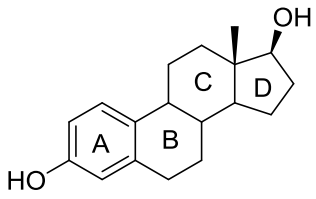

17β-Estradiol (E_2)

Figure 2. Immunofluorescent ERα degradation assay in MCF-7 breast cancer cell lines[a]

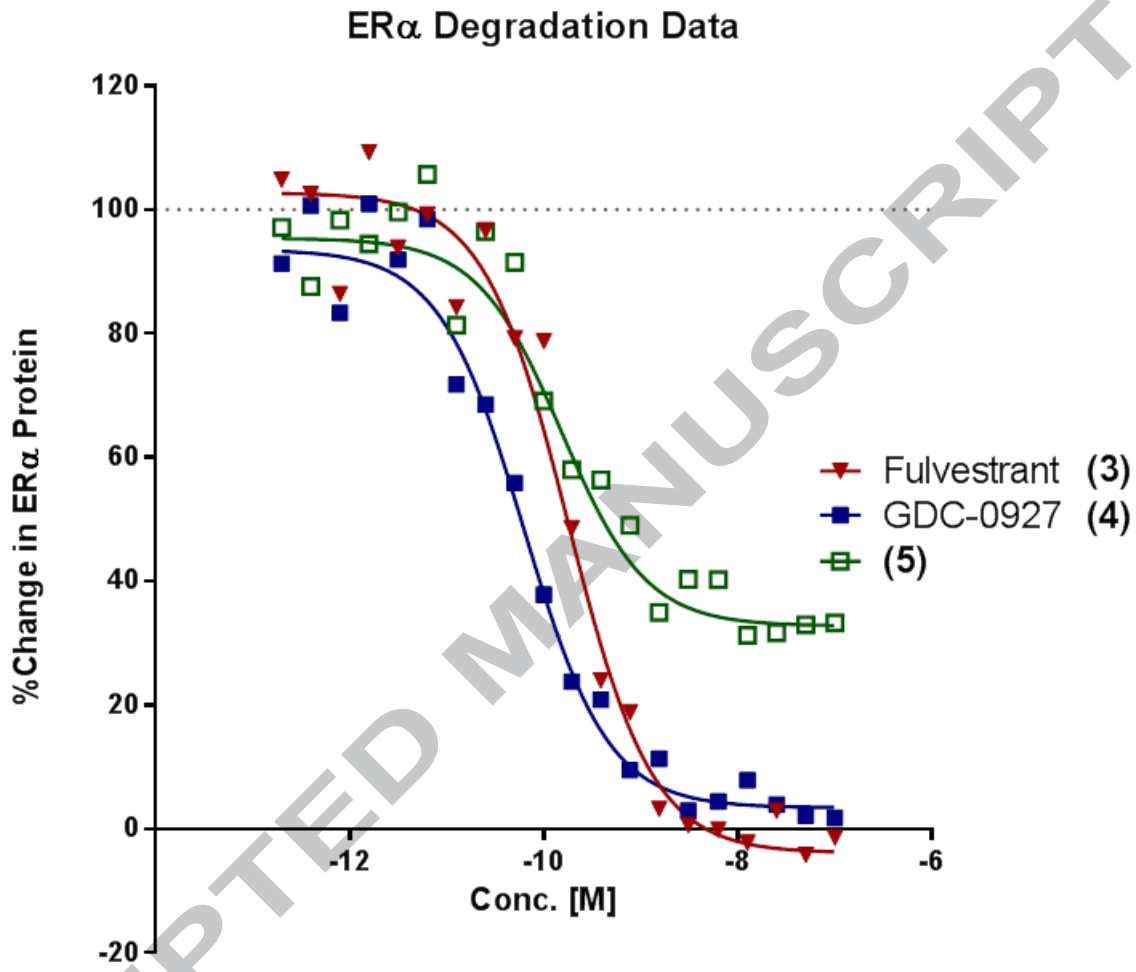

[a]: MCF-7 breast cancer cells in phenol-red free RPMI medium containing 10% charcoal stripped FBS; readings taken after 4 hours of compound incubation using an ERα-binding antibody (ESR1mAb F10) and quantitated with fluorescence imaging. The "Robust Fit" method was used to define the inflection point of curve (IC_{50}), the plateau of the maximal effect (S_{inf}) with DMSO and 5 nM fulvestrant treated samples being used to define 0% and 100% changes in ERα (see Supplementary Method 1 for assay details).

Tetracyclic compounds **16-19** were prepared according to a reported method[10] (Scheme 1). A modified Perkins reaction of a mixture of hydroxyacetophenones **6a-b** and substituted phenylacetic acids **7a-b** in the presence of trimethylamine in refluxing acetic anhydride afforded

coumarines **8a-d**. Homologation was achieved by reaction of the lithium homoenolate of **8a-d** with MOMCl. Global de-methylation using BBr_3 followed by cyclization under Mitsunobu conditions gave **11a-d**. The phenolic hydroxyl groups in **11a-d** were protected as *tert*-butyldimethylsilyl (TBDMS) derivatives **12a-d**. Reduction of **12a-d** with DIBAL-H cleanly afforded lactols **13a-d**. Addition of an organolithium derivative of the aminoalkoxybenzene **14** to lactols **13a-d** opened up the pyran B ring to afford a diol intermediate, which was subsequently cyclized to chromenes **15a-d** by treatment with concentrated HCl. Removal of the silyl protecting groups with tetrabutylammonium fluoride (TBAF) furnished target compounds **16-19** as racemic mixtures, which were separated by chiral supercritical fluid chromatography (SFC) into pure enantiomers.

Scheme 1.

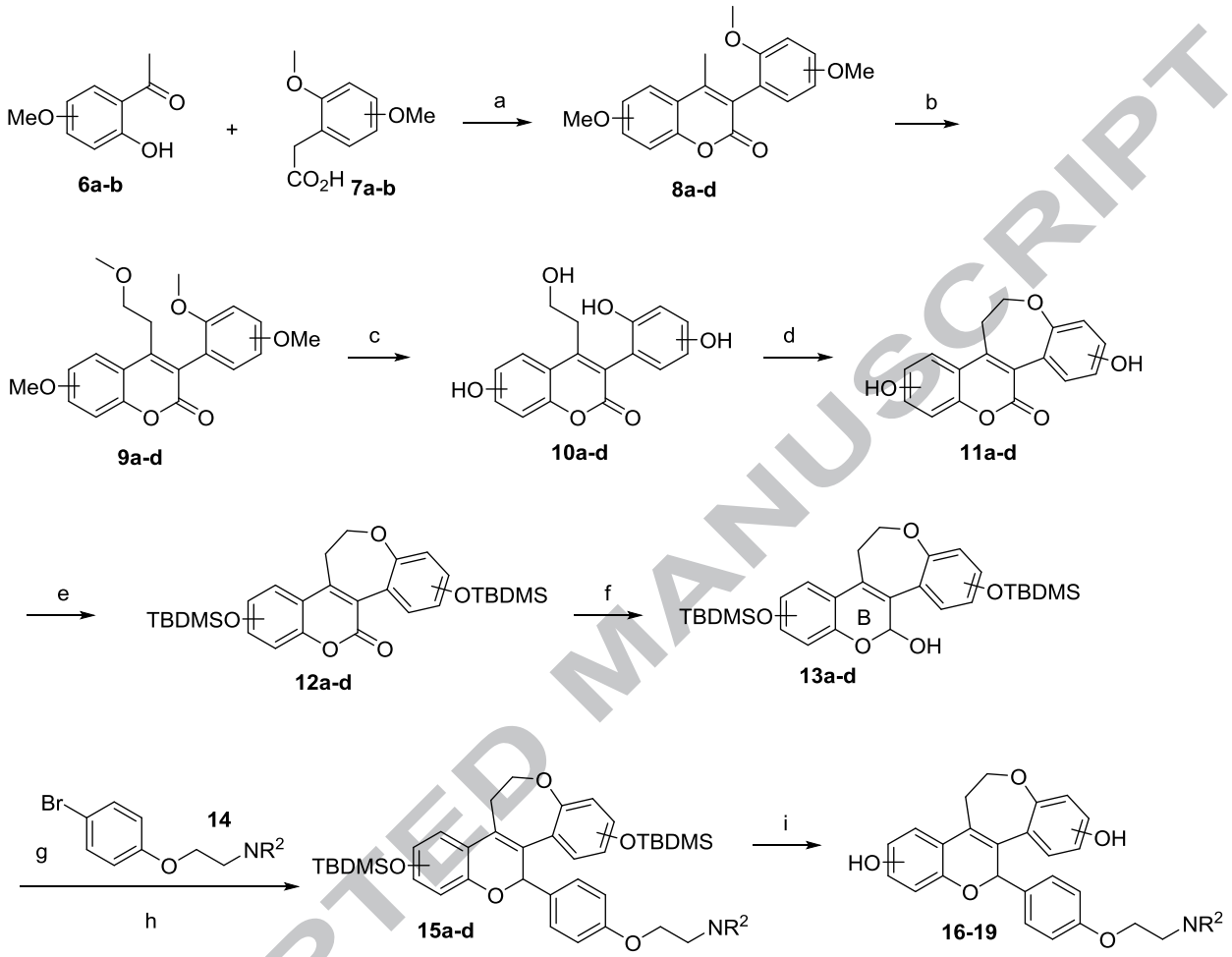

Reagents and conditions: (a) Ac_2O, Et_3N, reflux, 36 h, 42-52%; (b) LiHMDS, MOMCl, THF -78 °C to 0 °C, 70-99%; (c) BBr_3, DCM, 0 °C to rt, 82-90%; (d) diethylazidodicarboxylate, PPh_3, THF, rt, 20-60%; (e) TBDMSCl, DCM, rt, 58-88%; (f) DIBAL-H, DCM, -78 °C, 90-97%; (g) *n*BuLi, THF, -78 °C; (h) conc. HCl, DCM, 0 °C, 58-70% over 2 steps; (i) TBAF, THF, rt, 26-37%.

Previous results showed that fluoromethyl substituents on either the azetidine or pyrrolidine rings at the terminus of an ethoxy linker were optimal for maximizing ERα degradation for the chromene scaffold found in **4**.[9] Incorporation of a fluoromethyl substituted azetidine or pyrrolidine into a tetracyclic scaffold led to compounds **16a-c** (Table 1), resulting in

a significant improvement in ERα degradation potency and efficiency compared to **5** (IC_{50}: 0.045 – 0.076 nM, S_{inf}: 96-98% vs IC_{50}: 0.28 nM, S_{inf}: 64%). In fact, the degradation efficiency of **16a-c** was comparable to **4** (S_{inf}: 97%). It was also noteworthy that the anti-proliferative potency against MCF-7 breast cancer cell lines trends with ERα degradation potency, with **16a-c** (IC_{50} < 0.7 nM) displaying increased potency over **5** (IC_{50} = 1.2 nM). The fluoromethyl azetidine side chain in **16a** was selected over the fluoromethyl pyrrolidine in **16b-c** for further SAR investigation and profiling due to the reduced number of stereocenters and ease of synthesis (fluoromethyl azetidine commercially available).

Table 1. Evaluation of basic amine sidechains

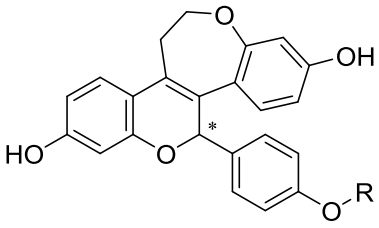

Compound	R	ERα Degradation[a]		MCF-7 Proliferation[c]
		IC_{50} (nM)	S_{inf} (%)[b]	IC_{50} (nM)
4	N/A	0.03	97	0.2
5-(±)	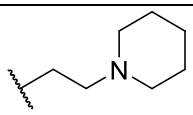	0.28	64	1.2
16a-(±)	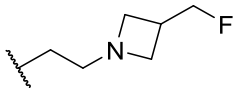	0.045	96	0.7
16b[d]	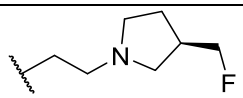	0.076	98	0.3
16c[d]	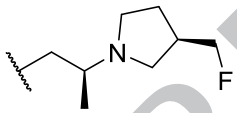	0.051	97	0.2

[a]: MCF-7 breast cancer cells in phenol-red free RPMI medium containing 10% charcoal stripped FBS; readings taken after 4 hours of compound incubation using an ERα-binding antibody (ESR1mAb F10) and quantitated with fluorescence imaging. The "Robust Fit" method was used to define the inflection point of curve (IC_{50}) and the plateau of the maximal effect (S_{inf}) with DMSO and 5 nM fulvestrant treated samples being used to define 0% and 100% changes in ERα (see Supplemental Method 1 for assay details). [b]: Recorded as a percentage of the curve plateau of fulvestrant at 5 nM as a control. [c]: MCF-7 proliferation assay in RPMI medium containing 10% FBS; 3-day incubation (see Supplementary Method 2 for assay details). [d]: mixture of diastereomers

In the constrained chromene structure and activity relationship (SAR) reported earlier, only a small number of enantiomeric pairs exhibited equivalent potencies in antagonist assays (ERα binding and MCF-7 proliferation), without structural rational being provided.[10] However, in the chromene core SAR, all enantiomeric pairs showed significant difference in degradation potency, while with similar S_{inf} value.[9] We separated racemic compound **16a** by chiral SFC into two enantiomers, **16aa** and **16ab**. To our surprise, enantiomers **16aa** (IC_{50}: 0.055 nM) and **16ab**

(IC_{50}: 0.059 nM) were nearly equipotent in the ERα degradation assay with **16aa** being a slightly better degrader (Table 2: S_{inf}: 96% vs 93% for **16aa** and **16ab**, respectively). The anti-proliferative potencies of enantiomers **16aa** (IC_{50}: 0.4 nM) and **16ab** (IC_{50}: 0.9 nM) were also nearly identical considering the assay variability (2-3 fold).

Table 2. Potencies of single enantiomers of 16a

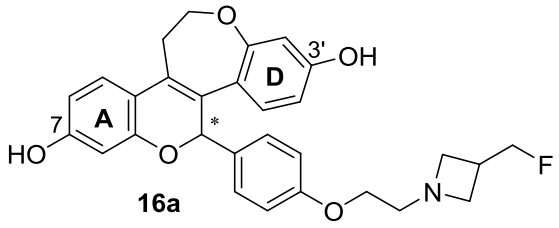

16a

Compound	ERα Degradation[a]		MCF-7 Proliferation[c]
	IC_{50} (nM)	S_{inf} (%)[b]	IC_{50} (nM)
16aa (*S*)	0.055	96	0.4
16ab (*R*)	0.059	93	0.9

[a]: MCF-7 breast cancer cells in phenol-red free RPMI medium containing 10% charcoal stripped FBS; readings taken after 4 hours of compound incubation using an ERα-binding antibody (ESR1mAb F10) and quantitated with fluorescence imaging. The "Robust Fit" method was used to define the inflection point of curve (IC_{50}), the plateau of the maximal effect (S_{inf}) with DMSO and 5 nM fulvestrant treated samples being used to define 0% and 100% changes in ERα (Supplementary Method 1). [b]: Recorded as a percentage of the curve plateau of fulvestrant at 5 nM as a control. [c]: MCF-7 proliferation assay in RPMI medium containing 10% FBS; 3-day incubation (see Supplementary Method 2 for assay details).

To gain insight into this interesting observation, we obtained X-ray crystal structures of the enantiomers in complex with the ERαLBD. The structures of the complexes were determined at 2.2 Å and 2.6 Å resolution for **16aa** and **16ab,** respectively (Figure 3). The co-crystal structures revealed that the more active enantiomer **16aa** possesses the (*S*)-absolute configuration and binds to ERαin the expected orientation. The phenolic hydroxyl 7-OH on the A-ring hydrogen bonds with Glu353 and Arg394, while the 3′-phenol on the D-ring forms a hydrogen bond with His524 (Figure 3a). On the other hand, the enantiomer **16ab**, which possesses the (*R*)-absolute configuration, binds to ERαin a "flipped" mode, with the 3′-phenol on the D-ring forming hydrogen bonds with Glu353 and Arg394, while the chromene 7-phenol on the A-ring forms a hydrogen bond with His524 (Figure 3b). In both cases, the basic side-chains of **16aa** and **16ab** adopt similar positions (Figure 3d); however, local disorder of the **16aa** tail and the adjacent protein sequence between helices 11 and 12 were poorly ordered. By contrast, this region is better defined in the **16ab** complex, and a hydrogen bond between the azetidine nitrogen and the sidechain of Glu353 is observed. To the best of our knowledge, this flipped A- and D-ring binding mode of a chromene with ERαhas not been reported and in our case readily explains the

equivalent potency of the enantiomers in the ERα degradation and MCF-7 anti-proliferation assays. This unexpected result shows that pseudo-symmetry of this template can bind in different modes within the ERαLBD.

Figure 3. Structures of **16aa** (**a**) (PDB code 6DFN) and **16ab** (**b**) (PDB code 6DF6) bound at the ERα LBD site. Dotted lines denote hydrogen bonds between ligand and protein. Amino acids within van der Waals distance of the ligand are shown, with key amino acids and structural elements labeled. The loop connecting Helix 11 and Helix 12 is disordered and/or destabilized by the ligand tail. Some portions of the protein, including regions interacting with Helix 12, were removed for visual clarity. (**c**) Interior binding site molecular surface of the crystal structures of **16aa** (yellow) and **16ab** (magenta) reveal that binding of the two different compound cores required no substantive conformational changes of the protein (only three fiducial protein sidechains shown). (**d**) Overlay of **16aa** (yellow) and **16ab** (magenta) based on protein coordinates. Their superposition reveals that their cores sweep out different space, yet their sidechains align well. Differences in position of the termini of the basic amine sidechains occur in areas of weak electron density and are consistently observed across crystal structures of similar compounds (data not shown).

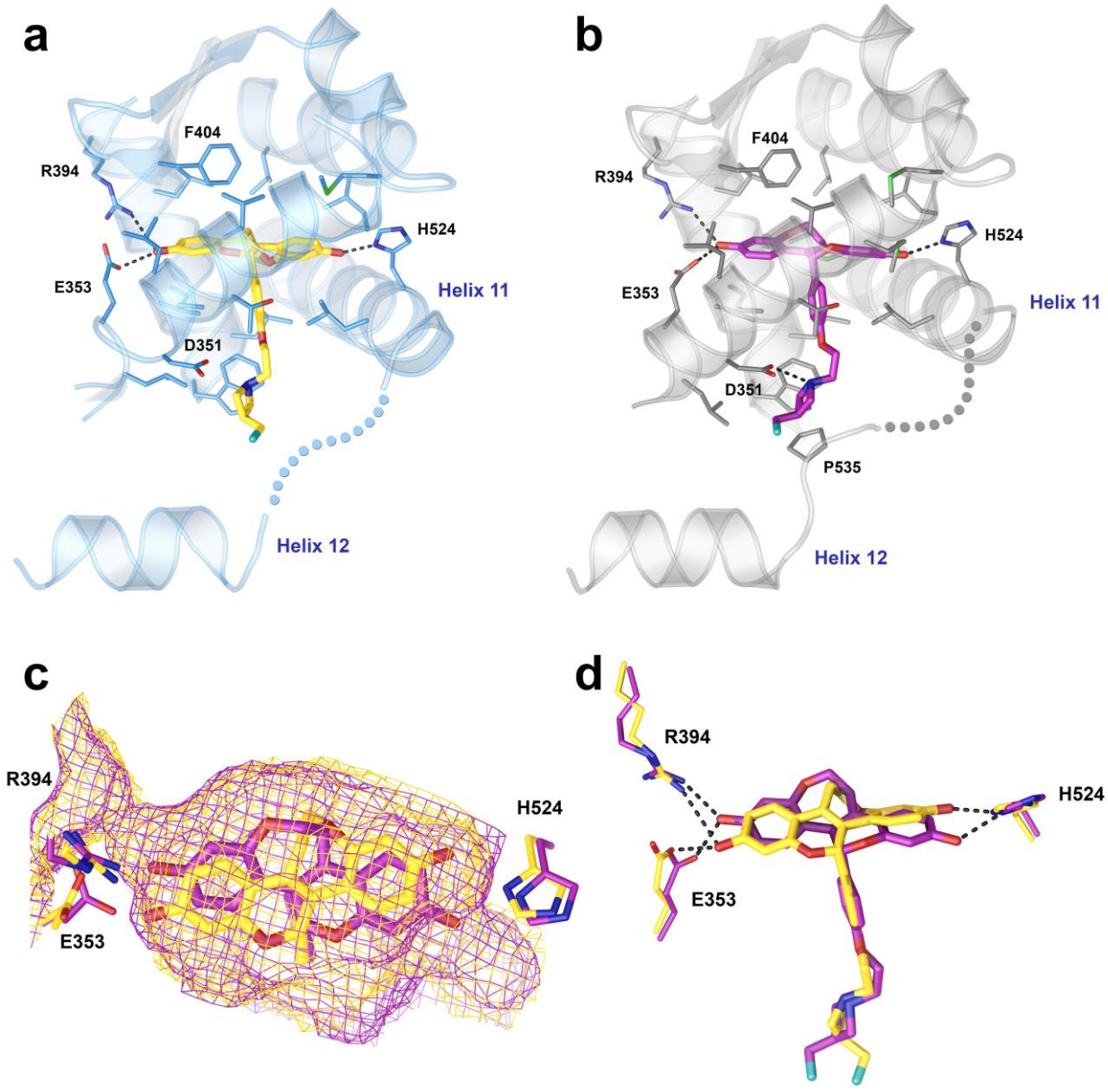

More recently, reports on related chromene systems have shown that the position of the hydroxy on the core can have an unexpected yet dramatic effect on potency and PK properties.[11] Therefore, we systematically examined the effect of the hydroxy's position by preparing three additional pairs of enantiomers **17a**-**19a** and **17b**-**19b** (Table 3). The **17a** / **17b** pair containing 6-OH and 3′-OH groups again demonstrated high and equivalent potency and efficiency in the ERα

degradation assay, similar to the **16aa** / **16ab** pair. Interestingly, for the other two pairs of enantiomers with a 4′-OH group on the D-ring, one enantiomer (**18a** and **19a**) was about 10-fold more potent than the matching enantiomers (**18b** and **19b**) in the ERα degradation and MCF-7 proliferation assays. The more potent enantiomers with a 4′-OH on the D-ring showed 10-fold reductions in ERα degradation potencies compared to their 3′-OH counterparts (**18a** vs **16aa**, **19a** vs **17a**). In summary, 3′-OH substitution on the D-ring seems to be optimal for high potencies for either binding mode. Once again, the anti-proliferation potencies tracked well with the ERα degradation potencies for all compounds listed.

Table 3. Evaluation of hydroxyl positions on the A- and D-rings

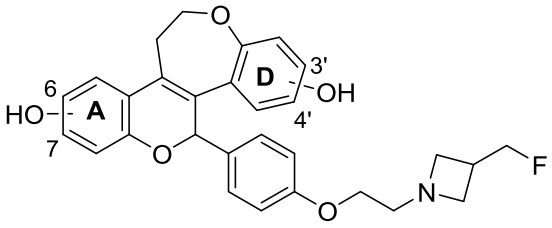

Compound	A-ring	D-ring	ER Degradation[a]		MCF-7 Proliferation[c]
			IC_{50} (nM)	S_{inf} (%)[b]	IC_{50} (nM)
16aa (*S*)	7-OH	3′-OH	0.055	96	0.4
16ab (*R*)	7-OH	3′-OH	0.059	93	0.9
17a (enant 1)	6-OH	3′-OH	0.021	98	0.3
17b (enant 2)	6-OH	3′-OH	0.024	100	0.6
18a (enant 1)	7-OH	4′-OH	0.61	90	5
18b (enant 2)	7-OH	4′-OH	9.6	85	20
19a (enant 1)	6-OH	4′-OH	0.24	93	0.8
19b (enant 2)	6-OH	4′-OH	3.2	100	10

[a]: MCF-7 breast cancer cells in phenol-red free RPMI medium containing 10% charcoal stripped FBS; readings taken after 4 hours of compound incubation using an ERα-binding antibody (ESR1mAb F10) and quantitated with fluorescence imaging. The "Robust Fit" method was used to define the inflection point of curve (IC_{50}), the plateau of the maximal effect (S_{inf}) with DMSO and 5 nM Fulvestrant treated samples being used to define 0% and 100% changes in ERα (Supplementary Method 1). [b]: Recorded as a percentage of the curve plateau of fulvestrant at 5 nM as a control. [c]: MCF-7 proliferation assay in RPMI medium containing 10% FBS; 3-day incubation (see Supplementary Method 2 for assay details).

We then proceeded to examine the metabolic stability of a few selected ligands *in vitro* (Table 4). All compounds were found to be labile upon incubation with rat hepatocytes, possibly due to a couple of reasons: 1) the measured lipophilicities of all compounds were high (LogD 2.7–3.2), suggesting that the compounds might be prone to oxidative metabolism; 2) the phenol hydroxy had extensive sulfation and glucuronidation. Indeed, when tested *in vivo*, compounds **4**,

16aa, **17a-b** all showed high clearance in rat, consistent with *in vitro* hepatocyte stability prediction. Additionally, **16aa** had poor oral bioavailability.

Table 4. Physicochemical properties, rat in vitro and in vivo PK for selected analogs

Compound	Rat Hep CLhep (mL/min/kg)[a]	Rat In Vivo CL (mL/min/kg)[b]	%F[b]	LogD[c]
4	46	85	16	2.9
16aa	36	57	3.2	3.0
16ab	27	ND	ND	3.2
17a	31	140	ND	2.7
17b	31	237	ND	2.7

[a]: Hepatic clearance predicted from hepatocytes. [b]: Female Sprague Dawley rats were given an intravenous dose of 1 mg/kg in 10/60/30 DMSO/PEG400/H_2O as a solution and an oral dose of 1 mg/kg in MCT as a suspension. [c]: Measured log of distribution coefficient between octanol and aqueous pH 7.4 buffer

We assessed the pharmacology of **16aa** in an ER responsive tissue utilizing a 4-day immature rat uterine wet weight (UWW) assay.[12] The assay was run in an antagonist mode in which the ligand competes against ethynyl estradiol, an agonist of ERα. Tamoxifen (a SERM) and **4** (a SERD) were included as positive controls in this assay. Tamoxifen had 36% reduction of uterine wet weight at a dose of 60 mg/kg, while **4** achieved 105.7% reduction at a dose of 10 mg/kg. Reduction of uterine wet weight was observed in a dose-responsive fashion for **16aa** (17% for 0.1 mg/kg vs 87% for 10 mg/kg, Figure 4). The plasma concentration of **16aa** at 4-hour time point was lower than that of **4**, which may help explain the smaller reduction in uterine wet weight (87% vs 105.7%).

Figure 4. Immature rat uterine wet weight assay in an antagonist mode[a]

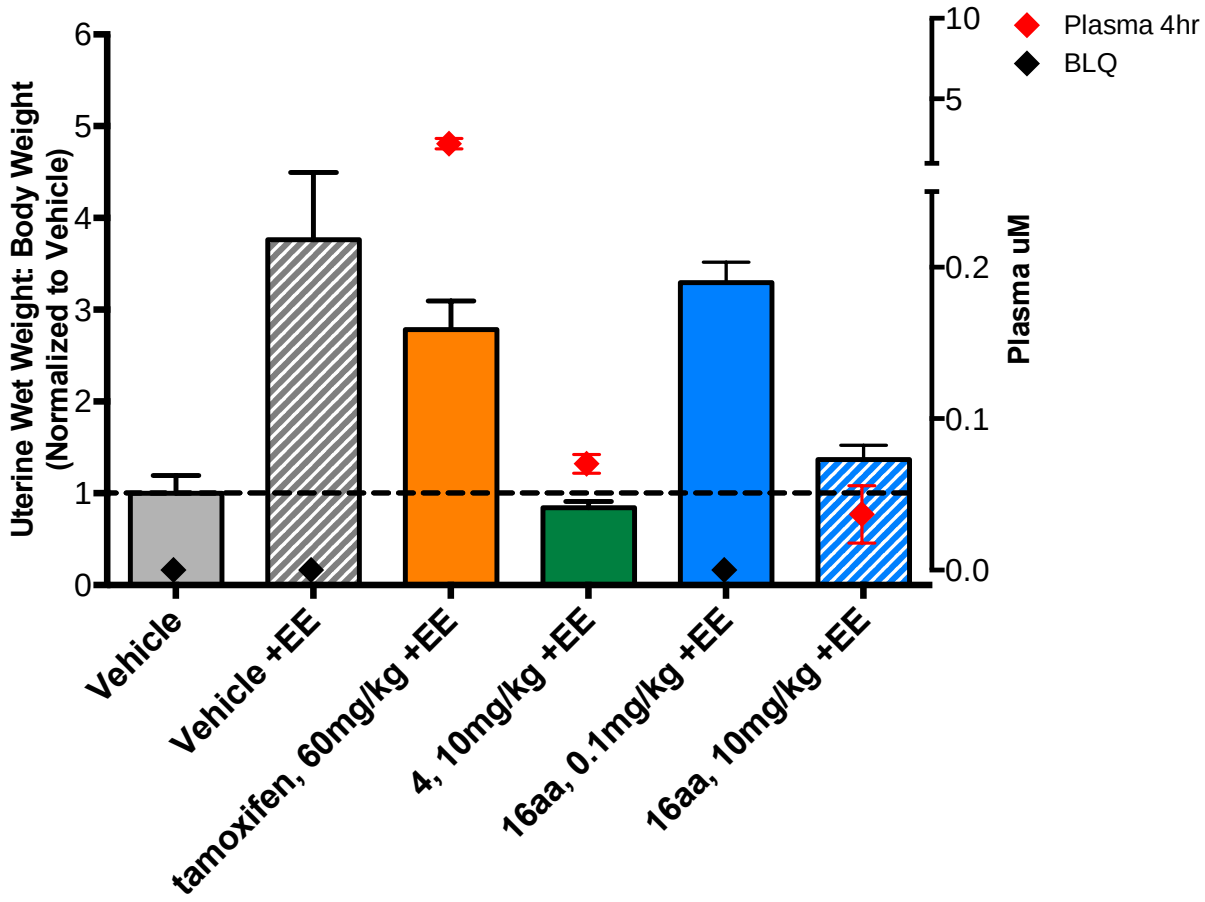

[a]: Compounds administered orally for 3 days (tamoxifen at 60 mg/kg, **4** at 10 mg/kg, **16aa** at 0.1, 10 mg/kg). On the fourth day, 24 hours after dose, the animals were euthanized. The uteri were collected, trimmed to 1 cm above uterine horn and weighed (see Supplementary Method 3 for assay details).

In summary, we investigated a SAR of tetracyclic benzopyranobenzoxepine analogs. Incorporating a fluoromethyl azetidine or fluoromethyl pyrrolidine side-chain led to highly potent and efficacious SERDs. The default and flipped binding mode of enantiomers **16aa** and **16ab** with ERα helped us rationalize the equivalent potency of **16aa** and **16ab** in the ERα degradation and MCF-7 anti-proliferation assays. Despite the excellent potency of **16aa**, further development was halted due to the poor pharmacokinetic profile of this class of molecules. Discovery of such a flipped binding mode may help design additional potent ERα ligands with unique structures.

ACKNOWLEDGEMENT

We thank the purification and analytical group, and the compound management group at Genentech for their support. We thank Joachim Rudolph for reviewing the manuscript. Research described in this paper was performed using beamline 08ID-1 at the Canadian Light Source, which is supported by the Canada Foundation for Innovation, Natural Sciences and Engineering Research Council of Canada, the University of Saskatchewan, the Government of Saskatchewan, Western Economic Diversification Canada, the National Research Council Canada, and the Canadian Institutes of Health Research. This research used data collected at beamline 5.0.2 of the Advanced Light Source, which is a DOE Office of Science User Facility under contract no. DE-AC02-05CH11231.

The crystal structures of 16aa and 16ab have accession codes 6DFN and 6DF6, respectively at the RCSB.

REFRENCES

1. McDonnell, D. P; Norris, J. D. *Science* **2002**, 296, 1642–1644.
2. Ariazi, E. A.; Jordan, V. C. *Nuclear Receptors as Drug Targets*; Ottow, E.; Weinmann, H., Eds. Wiley-VCH, **2008**, Vol. 39, 127–200.
3. Ariazi, E. A.; Ariazi, J. L.; Cordera, F.; Jordan, V. C. *Curr Top Med Chem* **2006**, 6, 181-202.
4. Nilsson, S.; Gustafsson, J. A. *Clin. Pharmacol. Ther.* **2011**, 89, 44-55.
5. Musgrove, E. A.; Sutherland, R. L. *Nat. Rev. Cancer* **2009**, 9, 631-43.
6. McDonnell, D. P.; Wardell, S. E.; Norris, J. D. *J. Med. Chem*. **2015**, 58, 4883–4887.
7. Johnston, S. J.; Cheung, K. L., *Curr. Med. Chem.* **2010**, 17, 902-914.

8. Ohno, S.; Rai, Y.; Iwata, H.; Yamamoto, N.; Yoshida, M.; Iwase, H.; Masuda, N.; Nakamura, S.; Taniguchi, H.; Kamigaki, S.; Noguchi, S. *Ann. Oncol*. **2010**, 21, 2342–2347.

9. Kahraman, M.; Govek, S. P.; Nagasawa, J. Y.; Lai, A., Bonnefous, C.; Douglas, K; Sensintaffar, J.; Lu, N.; Lee, K.; Aparicio, A.; Kaufman, J.; Qian, J.; Shao, G.; Prudente, R.; Joseph, J. D.; Darimont, B.; Brigham, D.; Heyman, R.; Rix, P. J.; Hager J. H.; Smith, N. D. *ACS Med. Chem. Lett.* **2019**, 10, 50-55.

10. Jain, N.; Xu, J.; Kanojia, R. M.; Du, F.; Guo, J.; Pacia, E.; Lai, M.; Musto, A.; Allan, G.; Reuman, M.; Li, X.; Hahn, D.; Cousineau, M.; Peng, S.; Ritchie, D.; Russell, R.; Lundeen, S.; Sui, Z. *J. Med. Chem*. **2009**, 52, 7544-7569.

11. (a) Kim, S.; Wu, J.; Chen, H. Y.; Birzin, E. T.; Chan, W.; Yang, Y. T.; Colwell, L.; Li, S.; Dahllund, J.; DiNinno, F.; Rohrer, S. P.; Schaeffer, J. M.; Hammond, M. L. *Bioorg. Med. Chem. Lett.* **2004,** *14*, 2741-2745. (b) Tan, Q.; Blizzard, T. A.; Morgan, J. D., 2nd; Birzin, E. T.; Chan, W.; Yang, Y. T.; Pai, L. Y.; Hayes, E. C.; DaSilva, C. A.; Warrier, S.; Yudkovitz, J.; Wilkinson, H. A.; Sharma, N.; Fitzgerald, P. M.; Li, S.; Colwell, L.; Fisher, J. E.; Adamski, S.; Reszka, A. A.; Kimmel, D.; DiNinno, F.; Rohrer, S. P.; Freedman, L. P.; Schaeffer, J. M.; Hammond, M. L. *Bioorg. Med. Chem. Lett.* **2005,** 15, 1675-1681.

12. Nagasawa, J.; Govek, S.; Kahraman, M.; Lai, A.; Bonnefous, C.; Douglas, K.; Sensintaffar, J.; Lu, N.; Lee, K.-J.; Aparicio, A.; Kaufman, J.; Qian, J.; Shao, G.; Prudente, R.; Joseph, J. D.; Darimont, B.; Brigham, D.; Grillot, K.; Heyman, R.; Rix, P.; Hager, J.; Smith, N. D. *J. Med. Chem.* **2018,** 61, 7917-7928.